



Steam-assisted synthesis of uniformly mesoporous anatase and its remarkably superior photocatalytic activities



Md. Kamal Hossain, Umme Sarmeen Akhtar, Agni Raj Koirala,
In Chul Hwang, Kyung Byung Yoon *

Korea Center for Artificial Photosynthesis, Center for Nanomaterials, Department of Chemistry, Sogang University, Seoul 121-742, Republic of Korea

ARTICLE INFO

Article history:

Received 25 June 2014

Received in revised form 19 July 2014

Accepted 22 July 2014

Available online 5 September 2014

Keywords:

Steam treatment

Large scale hexagonally ordered uniformly mesoporous anatase

Photocatalytic water reduction

4-Chlorophenol and methylene blue decompositions

ABSTRACT

The steam treatment of hexagonally ordered uniformly mesoporous (*h*-UM) amorphous TiO₂ at 120 °C for 1 h leads to highly crystalline *h*-UM anatase. This process is feasible for the large scale (>50 g) preparation. The surface area-normalized photocatalytic activities of *h*-UM anatase for water reduction and methylene blue and 4-chlorophenol decompositions are remarkably superior to those of wormhole-like randomly mesoporous anatase and anatase nanoparticles, demonstrating an important reason to prepare anatase in UM forms. Due to the extended crystalline interconnection, the band gap energy *h*-UM anatase decreases by 0.22 eV with respect to that of 25 nm anatase nanoparticle.

© 2014 Elsevier B.V. All rights reserved.

1. Introduction

Anatase, the most important polymorph of TiO₂, is one of the most important crystalline metal oxides which are currently widely used in industry and in academia for various purposes, in particular as photocatalysts. Anatase has usually been produced in three different forms, individual nanoparticles (NPs), randomly mesoporous (RM) anatase [1–7], and uniformly mesoporous (UM) anatase [8–34] (Fig. 1). The RM form is also called as wormhole-like randomly mesoporous (*w*-RM) anatase to emphasize the randomness of its pore systems [1–7]. The UM form can be further classified into hexagonally ordered uniformly mesoporous (*h*-UM) [8–13,16–26,28–34] and cubically ordered uniformly mesoporous (*c*-UM) [8–14,25–31] forms (Fig. 1). Recently, single crystalline randomly porous anatase has also been produced [35,36] but this is not a common form of anatase which is not covered in this work.

The NP form is the most frequently prepared form and the procedures to prepare it are well documented. *w*-RM anatase has usually been prepared by sintering the random aggregates of anatase NPs. Compared to those for NP and *w*-RM anatase, the preparation of UM anatase is much more difficult and the procedures are more complex. So far, three types of methods have been developed, which

are, soft template [8–25], hard template [8–13,25–31] and the combined assembly of soft and hard (CASH) template [8–13,32–34] methods. However, these methods have suffered the following drawbacks.

The critical drawback of the soft template method is that the crystallinities of the obtained UM anatase materials are poor, arising from the limitation of its crystallization temperature to ~400 °C, which is much lower than 550 °C, the minimum temperature required for the crystallization of the amorphous precursor to the crystalline anatase. Otherwise, thus if the crystallization temperature is increased higher than ~400 °C in the soft template method, the UM structure collapses. In the case of the hard template method the critical drawbacks are the very long and tedious procedures for the preparation of hard templates, the cumbersome removal of the hard templates which often involves the use of hydrofluoric acid, and the intrinsic difficulty to completely fill the pores of the hard template.

The CASH method is the most promising method to prepare UM anatase. Nevertheless, its drawback is that the crystallization temperatures (550–800 °C) [1,32–34] are too high from the energy saving and scale-up points of view. In this respect, the very low temperature (40 °C) method to prepare *h*-UM anatase films on substrates developed by Nilsson, Palmquist, and the co-worker [24] is quite impressive. Unfortunately, however, this method is limited to the preparation of thin *h*-UM anatase films of *h*-UM anatase on substrates but not for the preparation of bulk *h*-UM anatase. Thus, there

* Corresponding author. Tel.: +82 10 4041 6799; fax: +82 2 706 4269.

E-mail address: yoonkb@sogang.ac.kr (K.B. Yoon).

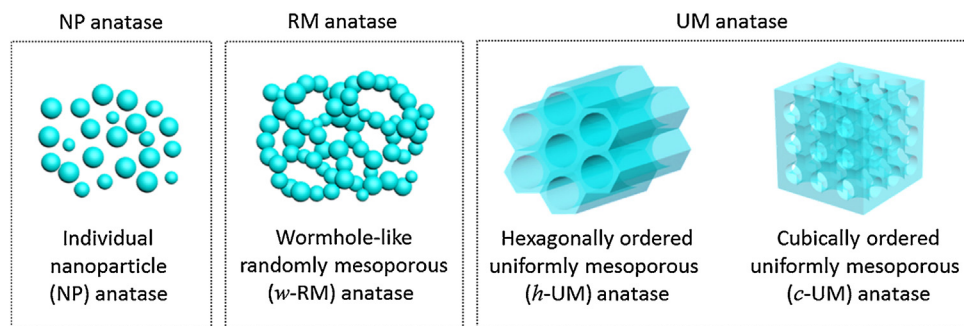


Fig. 1. Schematic illustrations of the three commonly prepared forms of anatase.

have been no mild temperature methods to prepare bulk *h*-UM anatase in large quantities. In this context, it is also worthwhile to note that in the case of *w*-RM anatase, there are several low temperature methods [2–5] including the one which yields *w*-RM anatase at room temperature, although it requires three months-long reaction periods [3]. Therefore, low temperature facile methods which are suitable for the production of UM anatase in large quantities have to be developed so that they can be more widely used for various research and applications.

Strangely, however, despite the aforementioned great efforts that have been made for the preparation of UM anatase, the reports that clearly describe the advantages of UM anatase over those of NP and *w*-RM anatase during the photocatalytic reactions are rare [25,27–29]. Even in such reports that deal with the advantages, it is not clear whether the superior photocatalytic activities of UM anatase come from their higher surface areas or from their intrinsic properties. In this respect, the genuine advantages or the intrinsic photocatalytic properties of UM anatase have to be elucidated so that it can be more extensively applied in various photocatalytic reactions.

We now report a novel low temperature method to prepare bulk UM anatase in large quantities and the genuine advantage of the UM anatase during photocatalytic reactions with respect to those of RM anatase and individual powder.

2. Experimental

2.1. Materials

Titanium isopropoxide [$>98\%$, $\text{Ti}(\text{OCH}(\text{CH}_3)_2)_4$, TIP] was purchased from Acros. Pluronic P123, methylene blue (MB), 4-chlorophenol and anatase nano-powder (NP, $<25\text{ nm}$) were purchased from Aldrich. P25 was purchased from Degussa and ST-01 from Ishihara Sangyo Kaisha, Ltd. Absolute ethanol, hydrochloric acid (HCl) and sulfuric acid (H_2SO_4) were purchased from Samchun. The reagents were used as received without further purification.

2.2. Synthesis procedure

The amorphous *h*-UM TiO_2 with the mesoporous walls lined with amorphous carbon was prepared according to the reported procedure [33]. The wall-lined *h*-UM TiO_2 was steam treated by placing them in an autoclave containing 0.5 mL of water and placing it in an oven preheated at 120°C for 1 h. The *h*-UM anatase whose mesopore walls were lined with carbon was calcined at 300°C for 5 h under oxygen or at 450°C under air for 5 h to produce highly crystalline mesoporous anatase. For the synthesis of *w*-RM TiO_2 , the surfactant-containing dry powder was calcined without annealing and steam treatment.

2.3. Measurements of photocatalytic activities

Hydrogen production experiments were performed in an airtight continuous flow stainless reactor connected with an online GC system (Young Lin, YL-6000) equipped with a flame ionization detector (FID), pulsed discharged detector (PDD). Typically, 0.1 g of an anatase sample was taken in a vial into which 20 mL of water and 4 mL of methanol was added. This vial was put into the above reactor and flushed with Ar (99.999%) with the flow rate of 6 mL/min for variable periods of time in the dark until the remnant air in the reactor disappeared. Then the sample was irradiated under the continuous flow of Ar with a standard AM-1.5 solar simulated light (HAL-302 Asahi) with the power of 72 mW cm^{-2} . The intensity of the light was adjusted using a one-sun checker (CS-20, Asahi Spectra Co., Ltd.). The area of irradiation was 6 cm^2 . The generated hydrogen gas was measured on-line equipped with a pulsed discharge detector (PDD) with Carboxen (Supelco) column and the amounts was reported in terms of nanomole (nmol) per unit area (1 cm^2) per h (nmol $\text{cm}^{-2}\text{ h}^{-1}$).

The photocatalytic degradations of methylene blue and 4-chlorophenol were carried out using a 200 W low pressure Hg lamp (Oriel CA-9015). Each catalyst (0.05 g) was introduced into an aliquot (50 mL) of a methylene blue solution (10 ppm, mg/L). Prior to irradiation, the heterogeneous solution was kept in the dark for 1 h with stirring to equilibrate the adsorption and desorption. The optical absorbance change of methylene blue solution was monitored at 660 nm and 4-chlorophenol was monitored at 225 nm.

2.4. Instrumentation

Small-angle X-ray (SAX) and wide angle X-ray (WAX) diffraction patterns of the samples were recorded on a Rigaku D/MAX-2500/pc diffractometer, using $\text{Cu-K}\alpha$ radiation (200 kV, 40 mA for WAX and 250 kV, 50 mA for SAX). N_2 sorption isotherms were measured at 77 K on a BELSORP-max. Prior to measurements, the samples were degassed under vacuum at 200°C for 6 h. The Brunauer–Emmett–Teller (BET) method was used to calculate the surface areas. The pore size distributions were obtained using the BJH method. Elemental analyses were performed on a Thermo Scientific Elemental Analyzer (Flash EA 1112 series). TEM images were recorded on a JEOL 2011 microscope operated at 200 kV. Diffuse-reflectance UV-vis spectra of the samples were recorded on a Varian Cary 5000 UV-vis-NIR spectrophotometer equipped with an integrating sphere. Barium sulfate was used as the reference. The diffuse reflectance spectra were converted into the Kubelka–Munk (K–M) formalism. The UV-vis absorption spectra of the methylene blue and 4-chlorophenol solutions were recorded on a diode array UV-vis Spectroscopy Scinco S-3100. The analyses of the hydrogen generated from water was performed on a gas chromatograph (GC, Young Lin, YL-6000) equipped with a flame ionization detector (FID) fitted with DB-624 column (Agilent), a pulsed discharged

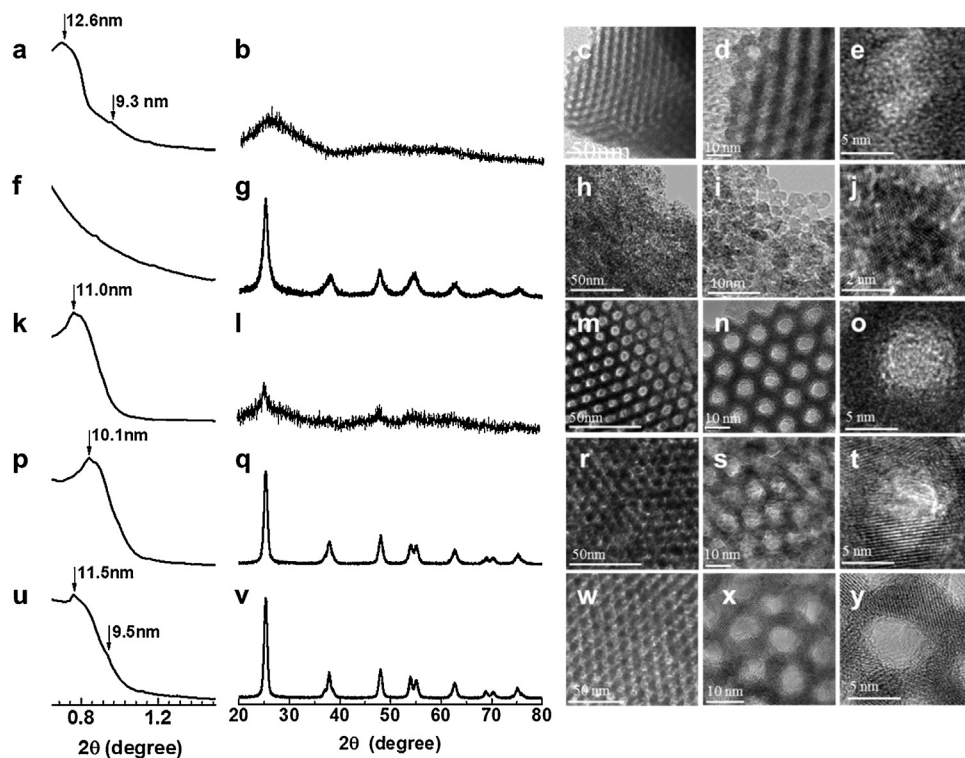


Fig. 2. SAX and WAX diffraction patterns and TEM images at various magnifications of amorphous *h*-UM TiO₂ after EISA (a–e), after steam treatment of the amorphous *h*-UM TiO₂ obtained by EISA at 120 °C for 1 h before carbonization (f–j), after carbonization of the amorphous *h*-UM TiO₂ obtained by EISA at 300 °C under N₂ for 1 h (k–o), after steam treatment of the carbonized amorphous *h*-UM TiO₂ at 120 °C for 1 h (p–t), and after calcination at 300 °C for 5 h under flow of O₂ (u–y), respectively.

detector (PDD) fitted with Carboxen column (Supelco), and a capillary injector.

3. Results and discussion

3.1. Synthesis and characterization

Using TIP as the Ti source, Pluronic P123 as the mesopore directing agent, the mixture of HCl and H₂SO₄, as the acid source, and ethanol as the solvent we prepared *h*-UM anatase. The routinely used scale was 12 g based on the weight of the obtained *h*-UM anatase. The ‘evaporation-induced self-assembly’ (EISA) [18,37] was carried out at 40 °C for 24 h. The small angle X-ray (SAX) diffraction pattern of the amorphous *h*-UM TiO₂ showed two diffraction peaks at $2\theta=0.70$ and 0.95° ($d=12.6$ and 9.3 nm, respectively) (Fig. 2a), demonstrating the presence of mesopores. However, the wide angle X-ray (WAX) diffraction pattern showed no peaks (Fig. 2b) confirming that the produced *h*-UM TiO₂ is amorphous. The transmission electron microscope (TEM) images of *h*-UM TiO₂ (Fig. 2c–e) also confirmed that it is mesoporous but not crystalline. When amorphous *h*-UM TiO₂ was steam treated at 120 °C for 1 h (step 1, Fig. 3), without prior carbonization of the organic template, w-RM anatase with the component crystal sizes of ~5 nm was produced. The SAX diffraction pattern showed the absence of the diffraction peaks (Fig. 2f). However, the broad shoulder indicated the presence of random mesoporosity. The broad WAX diffraction patterns showed that the newly produced material is very small crystalline anatase nanoparticles (Fig. 2g). The corresponding TEM images (Fig. 2h–j) clearly showed that the material is w-RM anatase with the component crystal sizes of ~5 nm. The obtained w-RM anatase still contained some aggregated surfactant, which disappeared upon calcining at 300 °C for 5 h under the O₂ flow (step 2, Fig. 3). The grain size still remained unchanged even after the calcination step.

The carbonization of the P123 aggregates was carried out at 300 °C for 1 h under the flow of N₂ (step 3, Fig. 3) according to a literature procedure [33]. After this step, the SAX diffraction peak shifted to a higher angle ($2\theta=0.77^\circ$, $d=11.0$ nm, Fig. 2k). The absence of diffraction peaks in WAX (Fig. 2l) and the corresponding TEM images (Fig. 2m–o) confirmed that this material is amorphous *h*-UM TiO₂.

After steam treatment at 120 °C for 1 h (step 4, Fig. 3), the SAX diffraction peak further shifted to a higher angle $2\theta=0.84^\circ$ ($d=10.1$ nm) (Fig. 2p). The WAX diffraction pattern showed the characteristic 11 peaks of the crystalline anatase (Fig. 2q). The TEM images (Fig. 2r–t) also confirmed the presence of hexagonally ordered mesopores and the characteristic lattice fringes of anatase. Thus, the steam treatment at 120 °C for 1 h not only induces the transformation of amorphous TiO₂ into pure crystalline anatase nanocrystals but also interconnection of them into stable *h*-UM anatase, which otherwise requires heating at the temperatures between 550 and 800 °C.

After removal of the wall-lining carbon in the *h*-UM anatase by calcination at 300 °C for 5 h under the flow of O₂ (step 5, Fig. 3), the SAX diffraction pattern showed two peaks at $d=11.5$ and 9.5 nm, respectively (Fig. 2u), and the intensities of the WAX diffraction peaks further increased (Fig. 2v) indicating the crystallinity of anatase has improved. The TEM images (Fig. 2w–y) further showed more vivid anatase lattice fringes. The sizes of the anatase grains in the *h*-UM anatase were 5–7 nm. The intensities of the SAX and WAX peaks remained the same even when the crystalline mesoporous anatase was heated at 650 °C for 2 h under the N₂ atmosphere, indicating its high thermal stability under the inert atmosphere. However, the intensity of the SAX peak decreased a bit and the WAX peaks became sharper upon heating at 550 °C for 2 h under the oxygen atmosphere, indicating that *h*-UM anatase is thermally less stable in the presence of molecular oxygen. The elemental analysis of *h*-UM anatase showed the absence of C and N. However it

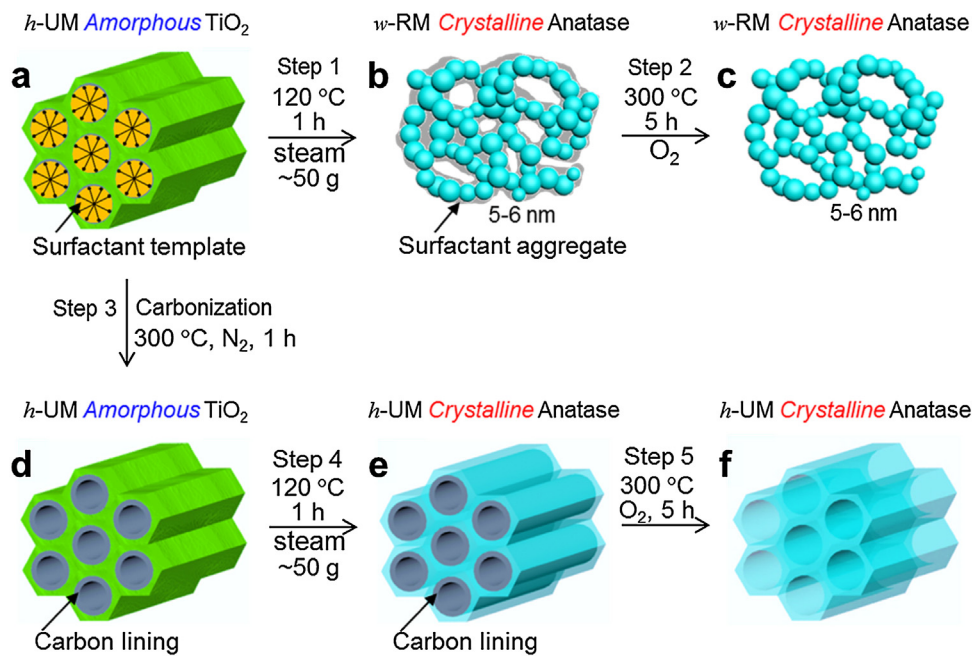


Fig. 3. Schematic illustration of the low-temperature steam methods to prepare *w*-RM and *h*-UM anatase.

contained a small amount of S (1.2%), which is likely to be arising from the unwashed H₂SO₄.

The type IV N₂ adsorption–desorption isotherms of the *w*-RM and *h*-UM confirmed their mesoporous natures (Fig. 4, left). The average pore sizes were 3–7 nm (Fig. 4, right). The surface areas of amorphous *h*-UM TiO₂ with surfactant aggregates (Fig. 3a), *w*-RM anatase with no surfactant aggregates (Fig. 3c), amorphous *h*-UM TiO₂ with carbon lining (Fig. 3d), *h*-UM anatase with carbon lining (Fig. 3e), and *h*-UM anatase (Fig. 3f) were 261, 173, 225, 185, and 169 m² g⁻¹, respectively. The corresponding pore volumes were 0.37, 0.17, 0.30, 0.28, and 0.26 cm³ g⁻¹, respectively. The average pore diameters are 5.1, 4.6, 5.4, 6.0, and 6.2 nm, respectively. Thus, we have successfully developed a novel, large scale method to crystallize the amorphous precursor to *h*-UM anatase under a mild (steam treatment at 120 °C) condition.

We found that the above procedure is also suitable for the preparation of *h*-UM anatase in a 50 g scale. The schematic illustration of this novel procedure is shown in (Fig. 3). Thus, our ‘low-temperature steam method’ has many advantages over the conventional ‘high-temperature dry method’.

To address the advantages of UM anatase over RM anatase and the individual anatase NPs during photocatalytic reactions we conducted photocatalytic reactions using five samples: *h*-UM anatase, *w*-RM anatase, individual anatase NPs, ST-01 and Degussa P25 NPs. The photocatalytic reactions were water reduction and decomposition of methylene blue (MB) and 4-chlorophenol (4-CP), respectively. As mentioned in the introductory part of this paper, previous reports on the superior photocatalytic [25,27,29] and electrocatalytic [30] activities of UM anatase did not take the surface area into consideration during the evaluation of their catalytic activities. We therefore compared the surface area-normalized catalytic activities of the five anatase species.

3.2. Photocatalytic H₂ production

The photocatalytic activities of the five samples for water reduction were compared under the one sun condition with methanol as the sacrificial electron donor (Fig. 6a). Because their surface areas were different (*h*-UM anatase = 169, *w*-RM anatase = 173, 25-nm anatase NPs = 55, ST-01 = 300, and Degussa P25 = 55 m² g⁻¹),

we normalized each H₂ yield with respect to the corresponding surface area. The surface area-normalized H₂ yield increases in the order: *h*-UM anatase ≫ *w*-RM anatase > Degussa P25 > 25-nm anatase > ST-01 NPs (Fig. 5a). The initially produced amounts of H₂ were 7.4, 0.36, 0.35, 0.13 and 0.12 nmol h⁻¹ cm⁻² m⁻². Thus, the surface area-normalized initial catalytic activity of *h*-UM anatase is ~21 times higher than that of *w*-RM anatase and Degussa P25, ~56 times higher than that of 25-nm anatase NPs and ~61 times higher than that of ST-01 NPs. This result thus shows another important reason to prepare anatase in a UM form but not a *w*-RM form. This result also opens the possibility to use *h*-UM anatase as novel visible light-utilizing photocatalysts for various reactions after doping with various co-catalysts. Although small, the catalytic activity of *w*-RM anatase is higher than that of 25-nm anatase, ST-01, and Degussa P25 NPs.

3.3. Photocatalytic degradation of methylene blue (MB)

The photocatalytic activities of the five samples on the decomposition of MB were compared under the UV-visible light (250–740 nm) generated from a 200W low pressure Hg lamp (Figs. 5b and 6b). The measured surface-area normalized first order decomposition rates (r/m²) were *h*-UM anatase = 21.3, 25-nm anatase NPs = 4.3, *w*-RM anatase = 2.6, ST-01 = 0.65, and Degussa P25 = 7.4 with the unit of 10⁻⁴ min⁻¹ m⁻². The intrinsic photocatalytic activity of *h*-UM anatase is higher than those of anatase NPs, *w*-RM anatase, ST-01 and Degussa P25 by 5, 8, 33 and 3 times, respectively. Thus, *w*-RM anatase shows the incomparably poorer photocatalytic activity than that of *h*-UM, indicating that some pores of *w*-RM anatase are too small for the large MB molecule to enter. This result again demonstrates why anatase should be prepared in the UM form but not in *w*-RM or NP form.

3.4. Photocatalytic degradation of 4-chlorophenol (4-CP)

The photocatalytic activities of the five samples on the decomposition of 4-CP were compared under the same UV-irradiation condition (Figs. 5c and 6c). In the absence of catalysts, 4-CP does not decompose at all under the experimental condition. The surface-area normalized first order decomposition rates (r/m²) were *h*-UM

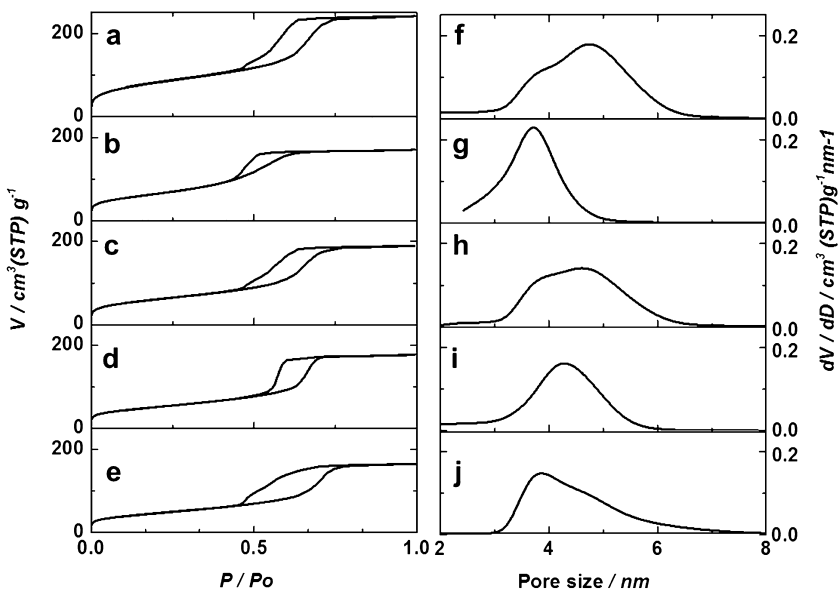


Fig. 4. N_2 adsorption–desorption isotherms (a–e) and pore size distributions (f–j) of amorphous *h*-UM TiO_2 after EISA (a and f), after steam treatment of the amorphous *h*-UM TiO_2 obtained by EISA at 120 °C for 1 h before carbonization (b and g), after carbonization of the amorphous *h*-UM TiO_2 obtained by EISA at 300 °C under N_2 for 1 h (c and h), after steam treatment of the carbonized amorphous *h*-UM TiO_2 at 120 °C for 1 h (d and i), and after calcination at 300 °C for 5 h under flow of O_2 (e and j).

anatase = 13.3, 25-nm anatase NPs = 2.9, *w*-RM anatase = 1.6, ST-01 = 0.3, and Degussa P25 = 3.71 in the unit of $10^{-4} \text{ min}^{-1} \text{ m}^{-2}$. Again, the photocatalytic activity of *h*-UM anatase is higher than those of anatase NPs and *w*-RM anatase by five and eight times, respectively.

The above results unambiguously demonstrate that the intrinsic photocatalytic activity *h*-UM anatase is much superior to those of *w*-RM anatase, 25-nm anatase NPs, ST-01, and Degussa P25. Now the above results clearly justify why the large scale economical methods to synthesize UM anatase should be developed so that it

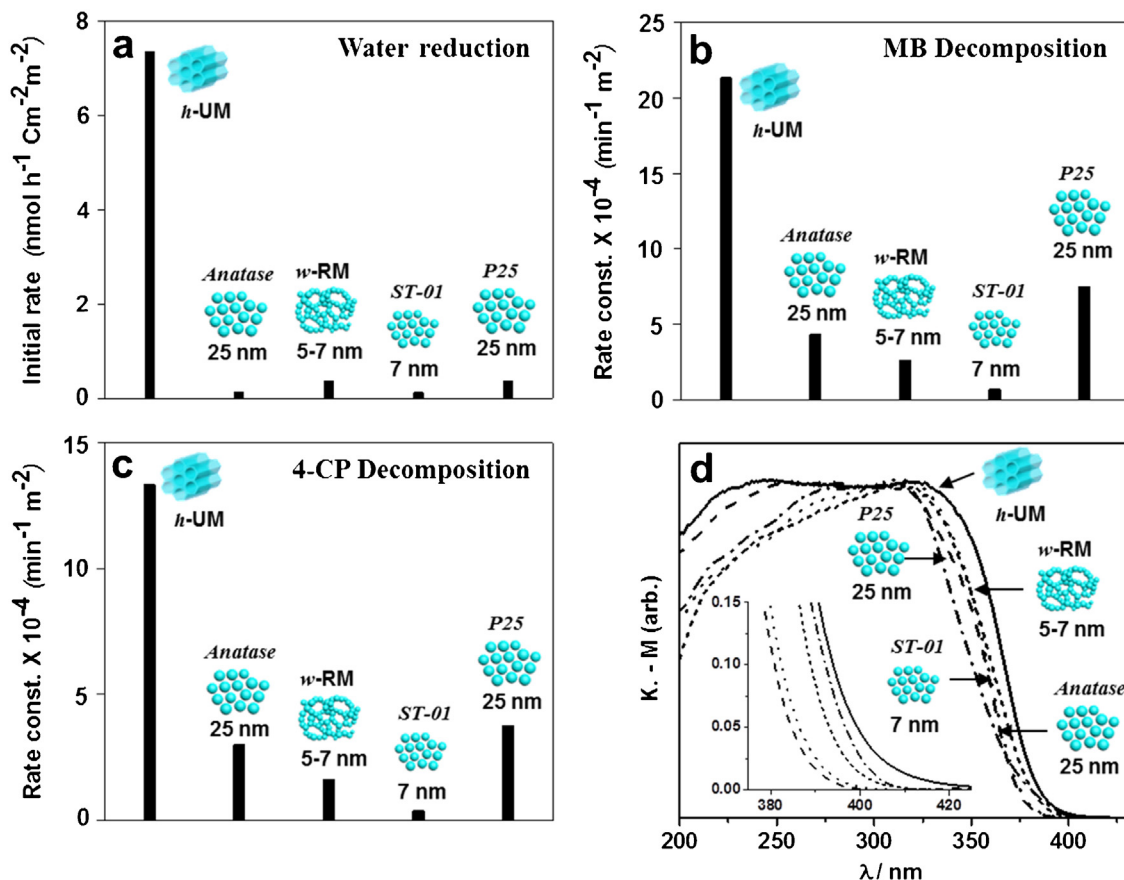


Fig. 5. Comparison of the photocatalytic activities of *h*-UM anatase, *w*-RM anatase, 25-nm sized anatase NPs, ST-01 and Degussa-P25 NPs for H_2 production from water (a), decomposition of MB (b), and 4-CP (c) and diffuse reflectance UV–vis spectra (d). The light source for water reduction was a solar simulated light.

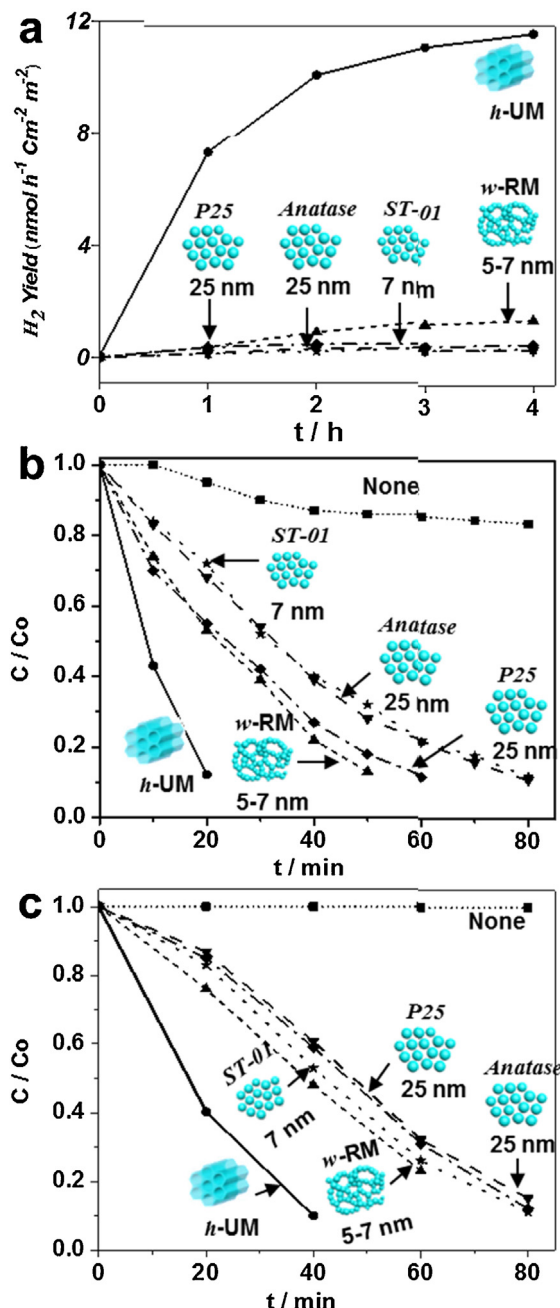


Fig. 6. (Raw data) Comparison of the photocatalytic activities of *h*-UM anatase, *w*-RM anatase, 25-nm sized anatase NPs, ST-01 and Degussa-P25 NPs for H₂ production from water (a), decomposition of MB (b) and 4-CP (c) respectively.

can be more widely used in various fields for various applications. In that sense, the facile '*large scale mild-temperature steam method*' introduced in this work is a highly valuable addition to the anatase and TiO₂ chemistry. Since this procedure is simple and requires only a mild reaction condition, the production of *h*-UM anatase is highly reliable and the physical properties of the produced *h*-UM anatase samples are the same regardless of the batch. We believe that *c*-UM anatase can be prepared similarly in large scales. The same methodology could be applied for the production of various other crystalline mesoporous metal oxides.

We attribute such remarkably superior catalytic activities of *h*-UM anatase over those of *w*-RM anatase to the following five special features which *w*-RM anatase cannot. Thus, the incorporated molecules have uniform diffusion rates within the UM

anatase due to the uniform channel size throughout the material (uniform diffusion rates). The diffusion rates of the incorporated molecules are faster in the UM anatase than in the *w*-RM anatase because the diffusion rate decreases if the channel size fluctuates (faster diffusion rates). The electronic and optical properties of the anatase wall and framework are constant arising from the uniformity of the anatase wall or framework thickness (constant electronic and optical properties). If a molecule once enters the UM anatase then all sites within it are accessible to the incorporated molecule, due to the complete openness of the channels from any entrance (complete pore openness). The transports of carriers (electrons and holes) along the wall or nanowire are faster in UM anatase than in *w*-RM anatase due to the three-dimensional (3D) crystalline interconnection of the anatase walls and nanowires (faster carrier transport rates), which is a very important requirement during the application of anatase for dye-sensitized solar cells and catalysis.

The intensity-normalized diffuse reflectance UV-vis spectra of the five anatase forms are compared in (Fig. 5d). Interestingly, while the onset of 25-nm sized anatase NP was 400 nm, that of *h*-UM anatase was 430 nm, despite the fact that the thickness of the *h*-UM anatase wall is only ~5 nm. This phenomenon seems to be arising from the crystalline interconnection between the component nanocrystals. In other words, *h*-UM anatase is a big polycrystalline anatase in which mesoporous channels run through. As a result, although the thickness is only ~5 nm, it is in fact a highly extended three-dimensional structure. Accordingly, the band gap energy decreases by 0.22 eV than that of 25-nm sized individual anatase NPs. This phenomenon is expected and is likened to the general phenomenon that, in a semiconductor, the increase in size leads to the decrease of the band gap energy. This is a novel addition to the intrinsic benefits of UM anatase.

4. Conclusions

The steam treatment of hexagonally ordered uniformly mesoporous (*h*-UM) amorphous TiO₂ at 120 °C for 1 h leads to highly crystalline *h*-UM anatase. This process is feasible for the large scale (>50 g) preparation. The surface area-normalized photocatalytic activities of *h*-UM anatase for water reduction and MB and 4-CP decompositions are remarkably superior to those of wormhole-like randomly mesoporous anatase, 25-nm anatase NPs, ST-01 and Degussa P25 NPs, demonstrating the important reason why anatase should be prepared in UM forms. Due to the extended crystalline interconnection, the band gap energy of *h*-UM anatase decreases by 0.22 eV with respect to that of 25 nm anatase nanoparticle.

Acknowledgements

This work was supported by the Korea Center for Artificial Photosynthesis, located at Sogang University and funded by the Ministry of Science, ICT and Future Planning through the National Research Foundation of Korea, No. 2009-0093886 and No. 2012R1A2A3A01009806. We also thank J.Y. Lee for the help in drawing figures and data compilation.

References

- [1] J. Lee, M.C. Orlall, S.C. Warren, M. Kamperman, F.J. Disalvo, U. Wiesner, *Nat. Mater.* 7 (2008) 222–228.
- [2] G.A. Seisenbaeva, G. Daniel, J. Nedelev, Y.K. Gun'ko, V.G. Kessler, *J. Mater. Chem.* 22 (2012) 20374–20380.
- [3] J. Su, X. Zou, G. Li, Y. Jiang, Y. Cao, J. Zhao, J. Chen, *Chem. Commun.* 49 (2013) 8217–8219.
- [4] P. Kohn, S. Pathak, M. Stefk, C. Ducati, U. Wiesner, U. Steinera, S. Guldin, *Nanoscale* 5 (2013) 10518–10524.
- [5] A. Hegazy, E. Prouzet, *Chem. Mater.* 24 (2012) 245–254.
- [6] I. Tamiolakis, I.N. Lykakis, A.P. Katsoulidis, G.S. Armatas, *Chem. Commun.* 48 (2012) 6687–6689.

- [7] L. Robben, A.A. Ismail, S.J. Lohmeier, A. Feldhoff, D.W. Bahnemann, J. Buhl, *Chem. Mater.* 24 (2012) 1268–1275.
- [8] R. Zhang, A.A. Elzatahry, S.S. Al-Deyab, D. Zhao, *Nano Today* 7 (2012) 344–366.
- [9] Y. Deng, J. Wei, Z. Sun, D. Zhao, *Chem. Soc. Rev.* 42 (2013) 4054–4070.
- [10] W. Li, Z. Wu, J. Wang, A.A. Elzatahry, D. Zhao, *Chem. Mater.* 26 (2014) 287–298.
- [11] D. Gu, F. Schüth, *Chem. Soc. Rev.* 43 (2014) 313–344.
- [12] A.A. Ismail, D.W. Bahnemann, *J. Mater. Chem.* 21 (2011) 11686–11707.
- [13] W. Zhou, H. Fu, *ChemCatChem* 5 (2013) 885–894.
- [14] D. Grosso, G.J. de A.A. Soler-Illia, E.L. Crepaldi, F. Cagnol, C. Sinturel, A. Bourgeois, A. Brunet-Brunneau, H. Amenitsch, P.A. Albouy, C. Sanchez, *Chem. Mater.* 15 (2003) 4562–4570.
- [15] M.H. Bartl, S.P. Puls, J. Tang, H.C. Lichtenegger, G.D. Stucky, *Angew. Chem. Int. Ed.* 43 (2004) 3037–3040.
- [16] K. Zimny, T. Roques-Carmes, C. Carteret, M.J. Stébé, J.L. Blin, *J. Phys. Chem. C* 116 (2012) 6585–6594.
- [17] D. Antonelli, J. Ying, *Angew. Chem. Int. Ed.* 34 (1995) 2014–2017.
- [18] P. Yang, D. Zhao, D.I. Margolese, B.F. Chmelka, G.D. Stucky, *Nature* 396 (1998) 152–155.
- [19] D. Li, H. Zhou, I. Honma, *Nat. Mater.* 3 (2004) 65–72.
- [20] C. Wu, T. Ohsuna, M. Kuwabara, K. Kuroda, *J. Am. Chem. Soc.* 128 (2006) 4544–4545.
- [21] D. Grosso, G.J. de A.A. Soler-Illia, F. Babonneau, C. Sanchez, P.A. Albouy, A. Brunet-Brunneau, A.R. Balkenende, *Adv. Mater.* 13 (2001) 1085–1090.
- [22] S.Y. Choi, M. Mamak, N. Coombs, N. Chopra, G.A. Ozin, *Adv. Funct. Mater.* 14 (2004) 335–344.
- [23] H. Shibata, T. Ogura, T. Mukai, T. Ohkubo, H. Sakai, M. Abe, *J. Am. Chem. Soc.* 127 (2005) 16396–16397.
- [24] E. Nilsson, Y. Sakamoto, A.E.C. Palmqvist, *Chem. Mater.* 23 (2011) 2781–2785.
- [25] M. Andersson, H. Birkedal, N.R. Franklin, T. Ostomel, S. Boettcher, A.E.C. Palmqvist, G.D. Stucky, *Chem. Mater.* 17 (2005) 1409–1415.
- [26] Z. Zhang, F. Zuo, P. Feng, *J. Mater. Chem.* 20 (2010) 2206–2212.
- [27] J. Wang, Z. Bian, J. Zhu, H. Li, *J. Mater. Chem. A* 1 (2013) 1296–1302.
- [28] W. Yue, X. Xu, J.S. Irvine, P. Attidekou, C. Liu, H. He, D. Zhao, W. Zhou, *Chem. Mater.* 21 (2009) 2540–2546.
- [29] Z. Bian, J. Zhu, J. Wen, F. Cao, Y. Huo, X. Qian, Y. Cao, M. Shen, H. Li, Y. Lu, *Angew. Chem. Int. Ed.* 50 (2011) 1105–1108.
- [30] Y. Ren, L.J. Hardwick, P.G. Bruce, *Angew. Chem. Int. Ed.* 49 (2010) 2570–2574.
- [31] W. Yue, C. Randorn, P.S. Attidekou, Z. Su, J.T.S. Irvine, W. Zhou, *Adv. Funct. Mater.* 19 (2009) 2826–2833.
- [32] W. Zhou, F. Sun, K. Pan, G. Tian, B. Jiang, Z. Ren, C. Tian, H. Fu, *Adv. Funct. Mater.* 21 (2011) 1922–1930.
- [33] R. Zhang, B. Tu, D. Zhao, *Chem. Eur. J.* 16 (2010) 9977–9981.
- [34] J. Zhang, Y. Deng, D. Gu, S. Wang, L. She, R. Che, Z. Wang, B. Tu, S. Xie, D. Zhao, *Adv. Energy Mater.* 1 (2011) 241–248.
- [35] E.J.W. Crossland, N. Noel, V. Sivaram, T. Leijtens, J.A. Alexander-Webber, H.J. Snaith, *Nature* 495 (2013) 215–219.
- [36] X. Zheng, Q. Kuang, K. Yan, Y. Qiu, J. Qiu, S. Yang, *Appl. Mater. Interfaces* 5 (2013) 11249–11257.
- [37] C.J. Brinker, Y. Lu, A. Sellinger, H. Fan, *Adv. Mater.* 11 (1999) 579–585.